β-Tubulin C354 Mutations that Severely Decrease Microtubule Dynamics Do Not Prevent Nuclear Migration in Yeast

Mohan L. Gupta, Jr.,* Claudia J. Bode,* Douglas A. Thrower,[†] Chad G. Pearson,[†] Kathy A. Suprenant,* Kerry S. Bloom,[†] and Richard H. Himes*[‡]

*Department of Molecular Biosciences, University of Kansas, Lawrence, Kansas 66045; and
[†]Department of Biology, University of North Carolina, Chapel Hill, North Carolina 27599

Microtubule dynamics are influenced by interactions of microtubules with cellular factors and by changes in the primary sequence of the tubulin molecule. Mutations of yeast β-tubulin C354, which is located near the binding site of some antimitotic compounds, reduce microtubule dynamicity greater than 90% in vivo and in vitro. The resulting intrinsically stable microtubules allowed us to determine which, if any, cellular processes are dependent on dynamic microtubules. The average number of cytoplasmic microtubules decreased from 3 in wild-type to 1 in mutant cells. The single microtubule effectively located the bud site before bud emergence. Although spindles were positioned near the bud neck at the onset of anaphase, the mutant cells were deficient in preanaphase spindle alignment along the mother-bud axis. Spindle microtubule dynamics and spindle elongation rates were also severely depressed in the mutants. The pattern and extent of cytoplasmic microtubule dynamics modulation through the cell cycle may reveal the minimum dynamic properties required to support growth. The ability to alter intrinsic microtubule dynamics and determine the in vivo phenotype of cells expressing the mutant tubulin provides a critical advance in assessing the dynamic requirements of an essential gene function.

INTRODUCTION

Microtubules are involved in essential cellular processes including chromosome movement during mitosis, vesicular trafficking, cellular polarization, and mRNA targeting. Microtubules are dynamic structures, i.e., at polymer mass steady state, individual microtubules are observed growing, depolymerizing, or remaining in a paused or attenuated state, in which no changes in microtubule length are observed (Mitchison and Kirschner, 1984). The dynamics of microtubules are controlled by a number of factors including microtubule-associated proteins (Drechsel *et al.*, 1992; Kowalski and Williams, 1993; Dhamodharan and Wadsworth, 1995; Hamill *et al.*, 1998), catastrophe-promoting proteins (reviewed in Walczak, 2000), motor proteins (reviewed in Hunter and Wordeman, 2000), and the GTPase activity of tubulin (reviewed in Erickson and O'Brien, 1992).

The subunit of microtubules, tubulin, is a heterodimer consisting of α- and β-tubulin. A number of biochemical studies have suggested that tubulin cysteine residues play roles in tubulin assembly into microtubules. For example, chemical modification of cysteine residues results in inhibition of tubulin assembly in vitro (Ludueña and Roach, 1991) and GTP hydrolysis by tubulin (Mejillano *et al.*, 1996). Cysteine residues can also be covalently cross-linked to the exchangeable site guanine nucleotide (Shivanna *et al.*, 1993; Jayaram and Haley, 1994; Bai *et al.*, 1999), to a colchicine analogue (Bai *et al.*, 1996) and to other antimitotic agents (Bai *et al.*, 1989; Shan *et al.*, 1999). Previously, we used site-directed mutagenesis to investigate the roles of the six cysteine residues in *Saccharomyces cerevisiae* Tub2p (β-tubulin) in the structure and function of tubulin (Gupta *et al.*, 2001). Of particular interest were the *tub2-C354S* and *tub2-C354A* mutations that produced phenotypes characteristic of greatly increased microtubule stability, including cold stability of microtubules and increased benomyl resistance (Gupta *et al.*, 2001). The increased stability could reflect alterations in the intrinsic properties of the microtubule or altered binding of regulatory proteins. The ability to correlate in vivo and in vitro dynamics allows us to distinguish these possibilities.

The budding yeast *S. cerevisiae* contains few microtubules compared with most other eukaryotic cells (Huffaker *et al.*,

1988), allowing one to dissect the contribution of microtubules and their dynamic properties to specific cellular events. The cytoplasmic microtubules are required for positioning the nucleus to the neck before anaphase onset, and contribute to spindle elongation in anaphase. The nuclear microtubules form the bipolar spindle and are required for chromosome segregation. It has been proposed that the highly dynamic nature of microtubules contributes to a search and capture mechanism of cytoplasmic microtubules at the site of bud growth during G1 (Carminati and Stearns, 1997; Shaw *et al.*, 1997b) and of nuclear microtubules at the kinetochores before chromosome segregation (Holy and Leibler, 1994; Winey *et al.*, 1995; O'Toole *et al.*, 1999; Maddox *et al.*, 2000). However, it has not been possible to distinguish the role of microtubule dynamics from the essential role of microtubules for cellular viability.

In this report we utilize two *tub2-C354* mutant strains that exhibit altered microtubule dynamics in vivo and in vitro. We find that cytoplasmic microtubule dynamics are greatly reduced. In addition, the number of cytoplasmic microtubules is reduced to approximately one per spindle pole body. Although this stable microtubule is able to locate the incipient bud site, the spindle is not aligned correctly along the mother-bud axis. Moreover, tubulin turnover in the nuclear spindle microtubules is reduced in the mutant strains. The defect in microtubule dynamics restricts the extent and rate of spindle elongation during anaphase. The cell cycle regulation of microtubule dynamics is also altered. In wild-type cells, microtubules are most dynamic in G1, whereas in the *tub2-C354* mutants, G1 dynamics in unbudded cells are reduced relative to budded cells. These studies reveal important roles of microtubule regulatory proteins throughout the cell cycle.

MATERIALS AND METHODS

Yeast Strains

The yeast strains used in this study were MGY1 (*MAT*a, *leu2Δ1*, *trp1Δ63*, *his4-917*, URA3/ura3-52, *tub2*-His$_6$), which contains a His$_6$ tag at the C terminus of Tub2p, and the MGY1 mutant strain MGY1-C354S (*MAT*a, *leu2Δ1*, *trp1Δ63*, *his4-917*, URA3/ura3-52, *tub2*-His$_6$-C354S; Gupta *et al.*, 2001). Also, created for this study were the strains FY41-GFP (*MAT*a, LEU2::GFP-TUB1::leu2Δ1, *trp1Δ63*, *his4-917*, ura3-52, TUB1, TUB2), which is FY41 (Davis *et al.*, 1993) containing the GFP-Tub1p fusion protein (described below) and the FY41-GFP mutant strains: FY41-GFP-C354A (*MAT*a, LEU2::GFP-TUB1::leu2Δ1, *trp1Δ63*, *his4-917*, URA3/ura3-52, TUB1, *tub2*-C354A) and FY41-GFP-C354S (*MAT*a, LEU2::GFP-TUB1::leu2Δ1, *trp1Δ63*, *his4-917*, URA3/ura3-52, TUB1, *tub2*-C354S), which are FY41-GFP containing the respective tub2p-C354 mutations (described below).

Construction of the GFP-Tub1p Strains

The plasmid pMG3 encoding GFP-Tub1p under control of the *TUB1* promoter was created by cloning the GFP-*TUB1* construct from pAFS125 (A. Straight, Harvard University, Cambridge, MA) into the multiple cloning site of the yeast integrating plasmid pRS405. The 3100-base pair *Kpn*I-*Sac*I fragment from pAFS125 containing GFP-*TUB1* and the endogenous *TUB1* promoter was combined with the 924-base pair *Kpn*I-*Kas*I and 4472-base pair *Kas*I-*Sac*I fragments from pRS405 in a three-way ligation reaction. When digested at the single *Kas*I site, pMG3 integrates at the *LEU2* locus.

The strain FY41-GFP was created by transforming FY41 with linearized pMG3. The mutant strains FY41-GFP-C354A and FY41-GFP-C354S were constructed by transforming FY41-GFP with the

transplacement fragment from pCS3 (Sage *et al.*, 1995a) containing a *tub2*-C354A or *tub2*-C354S mutation, respectively. All DNA manipulations, isolation of transformants, and verification of mutations were done as described previously (Gupta *et al.*, 2001).

In Vivo Microtubule Dynamics: Microscopic Imaging

Cells were grown to midlog phase and mounted as described previously (Yeh *et al.*, 1995; Maddox *et al.*, 2000) using SD-complete media (0.67% yeast nitrogen base without amino acids, 2% glucose, 0.5% casamino acids), and 50 μg/ml each uracil, tryptophan, and adenine. The equipment and techniques for imaging GFP-fusion proteins have been described in detail (Shaw *et al.*, 1997a). Cells were grown and maintained at 23°C during image acquisition. The typical acquisition protocol acquired five z-series fluorescent images at 0.75-μm axial steps and a single differential interference contrast (DIC) image corresponding to the central fluorescent image. Time-lapse image series, which were typically acquired at 8-s intervals for wild-type microtubules, were usually acquired every 20 s for *tub2-C354* mutant microtubules in order to extend the duration of the analysis. For microtubule dynamics analysis, time-lapse series lasted between 6 and 60 min. For spindle dynamics and cell cycle analysis, image sets were typically acquired every 60 s and the total series could cover >2 h before significant photobleaching occurred.

In Vivo Microtubule Dynamics: Image Analysis and Quantification

Yeast cells were segregated into four categories for in vivo microtubule dynamics analysis. Unbudded cells were single cells with no bud growth visible by DIC microscopy. Cells were classified as small-budded from the time an emerging bud became visible by DIC microscopy until duplicated spindle pole body separation became visible by fluorescence microscopy. The separation of duplicated spindle pole bodies was evident by two distinct dots of GFP-Tub1p fluorescence replacing the previously singular dot. Budded cells that had a bipolar spindle <2 μm in length were classified as preanaphase cells. Budded cells were identified as anaphase cells from the time the mitotic spindle had elongated to >2 μm in length until spindle midzone separation became visible.

Only microtubules and spindles whose entire length lay within the series of z-focal plane images were used for analysis. If possible, multiple cells from the same time-lapse series or multiple microtubules from a single cell were analyzed. In the case of the *tub2-C354A* mutant, and to a lesser extent the *tub2-C354S* mutant, cells were seen with deviations in cell morphology (Gupta *et al.*, 2001). Cells with individual characteristics not representative of the strain as a whole were not used for microtubule dynamics analysis.

At each time point, microtubules were analyzed by identifying the tip and the base of the microtubule in their respective z-plane images. The Cartesian coordinates and the z-plane separation distance of the microtubule ends were used to calculate the three-dimensional length of the microtubule. Each series of time-lapse images was analyzed three separate times as independent sets of measurements, which were used to construct microtubule lifetime history plots using the averages of the three length measurements.

Microtubule dynamics rates were calculated by linear regression analysis of the lifetime history plots. Growth and shortening events are defined as a set of at least four consecutive time-points with an R^2 value ≥0.85 and a length excursion ≥ 0.6 μm. Pause events are defined as at least four consecutive time-points during which length change was < ±0.2 μm. Because at least four consecutive time-points were considered in linear regression analysis, all growth, shortening, and attenuation events in wild-type and *tub2-C354* mutant cells lasted longer than 24 and 60 s, respectively. Catastrophe is defined as a transition to shortening after a period of growth or pause. Similarly, rescue is defined as a transition to growth following a period of pause or depolymerization. Brief periods in some of

the time-lapse series remained unclassified because they did not meet the criteria set for time duration, length of excursion, or statistical significance. The proportion of time spent in each phase was calculated by dividing the sum of the time spent in each phase by the total evaluated time for all microtubules observed. The frequencies of catastrophe and rescue were calculated by dividing the number of events observed by the total evaluated time. SDs were calculated as the frequencies of catastrophe or rescue divided by the square root of the number of events observed (Walker *et al.*, 1988). Microtubule dynamicity was calculated as the total number of tubulin dimers exchanged per microtubule end (using 1690 dimers/μm microtubule) considering the proportion of time spent in growth, shortening, or pause phase (Toso *et al.*, 1993).

The number of cytoplasmic microtubules was determined by GFP-Tub1p fluorescence using single time point *z*-series images. Fluorescent intensity line scan analysis (MetaMorph software) was performed on a three-pixel line along the length of microtubules that were contained within a single *z*-focal plane image. The gray-scale intensity values of each line scan were scaled to demonstrate relative changes in intensity.

Spindle Elongation, Position, and Orientation

Spindle length during elongation, from the outside edges of the spindle poles, was calculated in the same manner described for in vivo microtubule analysis and quantification. Spindle position was determined by measuring the distance from the outside edge of the bud-proximal spindle pole body to the center of the bud neck in two-dimensional *z*-series composite images ~1 min before the spindle elongated to >2 μm. To determine the angle of orientation for preanaphase spindles, time-lapse sequences were selected which displayed the complete spindle (<2 μm long) for at least 10 min. At 1-min intervals, the angle of a line intersecting both spindle poles was determined relative to the mother-daughter axis of the cell in two-dimensional *z*-series composite images. A total of 10, 13, and 15 spindle images were used to determine spindle orientation for wild-type, *tub2-C354S*, and *tub2-C354A* mutant strains, respectively.

FRAP Experiments

Fluorescence recovery after photobleaching (FRAP) experiments and statistical analysis were carried out as described in Maddox *et al.* (2000). Five 350-ms exposure images were acquired at each time point to create a through focus *z*-series stack with 30-s or 2-min intervals. The mitotic half-spindle was photobleached using a 35-ms laser exposure. The ratio of bleached:unbleached region after recovery R, first-order rate constant k, and half-time to recovery ($t_{1/2}$) were calculated at the following average time points: 2 min (FY41-GFP), 17.6 min (FY41-GFP-C354S), and 18.6 min (FY41-GFP-C354A).

Purification of Yeast Tubulin

Yeast strains MGY1 and MGY1-C354S were grown in 34 L of YPD medium (1% yeast extract, 2% peptone, 2% glucose) in 2–20 L carboys. After overnight growth at 30°C with vigorous aeration, the medium was supplemented with an additional 2% glucose, and the pH was adjusted to ~6.5 with 4 M NH$_4$OH. Growth was continued for an additional 5 h, and cells harvested in a Sharples Type T-1P continuous flow centrifuge (Pennwalt Corp., Warminster, PA). Approximately 500 g of packed, wet weight cells were obtained.

Wild-type cells were suspended in 100 ml of H-PEM (100 mM Pipes, 2 mM EGTA, 10 mM MgSO$_4$, pH 6.9) and stored at 4°C overnight. (In our previous article we found that it takes at least 6 h to completely depolymerize yeast cellular microtubules at 4°C [Gupta *et al.*, 2001]). Because incubation of MGY1-C354S cells at 4°C induces the formation of cold-stable tubulin polymers (Gupta *et al.*, 2001), these cells were suspended in H-PEM and processed immediately for tubulin purification. Immediately before purification, the total volume of H-PEM was brought to 750 ml and made 5 mM in
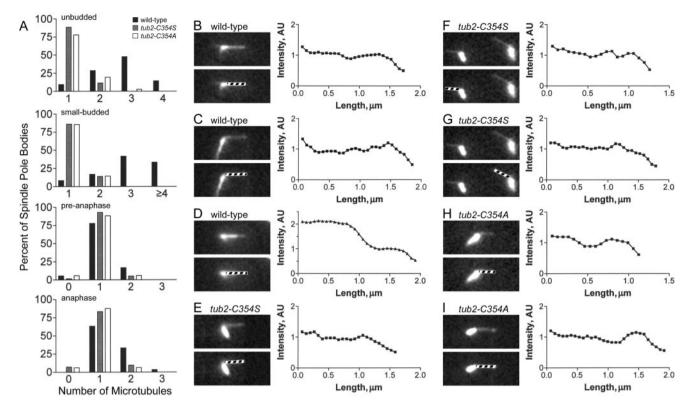
dithiothreitol, 2 mM in phenylmethylsulfonyl fluoride, and 0.1 mM in GTP. The cells were lysed by passing the suspension 10 times through a Microfluidizer 110-Y (Microfluidics Corp., Newton, MA) using an iced cooling coil. This method produced >95% cell breakage.

The initial stages of the purification procedure were based on the procedures of Barnes *et al.* (1992) and Davis *et al.*, (1993). All steps were done at 4°C. The lysed cells were centrifuged at 10,000 × g for 10 min, and the resulting supernatant was centrifuged at 100,000 × g for 60 min. The 100,000 × g supernatant was made 10% in glycerol and 0.16 M in NaCl. A 400-ml bed volume of DE52 (Whatman Inc., Fairfield, NJ), equilibrated with H-PEM + 0.16 M NaCl, was added as a 70% slurry, and the suspension was stirred gently for 45 min.

The DE52 was washed twice by centrifugation (7000 × g for 10 min) and resuspension in 600 ml PMG (100 mM Pipes, 1 mM MgSO$_4$, 10% gycerol, pH 6.9) containing 0.16 M NaCl, after which it was suspended in 300 ml of the same solution and loaded into a 30 × 5-cm column. After gravity packing, the column was washed with an additional 75 ml of the same solution. The majority of proteins were not retained by the resin. Remaining proteins were eluted with PMG25 (PMG with 25 mM Pipes) containing 0.5 M NaCl. Fractions containing protein, determined by the Bradford assay (Bradford, 1976), were pooled and brought to 20 mM imidazole using a 500 mM solution, and the pH was adjusted to 7.4 with NaOH. A 5-ml bed volume of Ni-NTA resin (Qiagen, Valencia, CA), washed twice in 50 ml PMG25 containing 20 mM imidazole and 0.5 M NaCl, pH 7.4, was added to the pooled fractions as a 50% slurry. The suspension was stirred gently for 45 min, and the Ni-NTA resin was collected by centrifugation for 7 min at 3000 × g. The resin was washed twice with 25 ml of the same solution followed by 15 ml of a solution containing 25 mM Pipes, 1 mM MgSO$_4$, 20 mM imidazole, pH 7.4. The resin was finally suspended in 3 ml of the latter solution and loaded into a 20 × 0.5-cm column. Proteins were eluted with 350 mM imidazole, pH 6.9, using a flow rate of 0.2 ml/min, and 0.5-ml fractions were collected. Tubulin eluted immediately following one void volume. Fractions containing >0.75 mg/ml tubulin were pooled and dialyzed twice for 45 min against 300 volumes of 10 mM Pipes, 0.1 mM EGTA, 0.1 mM MgSO$_4$, 50 μM GTP, pH 6.9, in a 10,000 MWCO Slide-A-Lyzer Cassette (Pierce Chemical Co., Rockford, IL). Fractions of ~0.2–0.75 mg/ml tubulin were pooled separately and dialyzed against PEM (100 mM Pipes, 1 mM EGTA, 1 mM MgSO$_4$, pH 6.9) containing 50 μM GTP. After dialysis the tubulin was centrifuged for 10 min at 100,000 × g, drop-frozen into liquid nitrogen, and stored at −80°C. The purification procedure produced 3–4 mg of tubulin from the wild-type strain. The yield from the MGY1-C354S strain was less because of the cold-stable nature of the microtubules in this strain.

In Vitro Microtubule Dynamics

Dynamics analyses of individual microtubules were performed using a nucleated assembly assay with purified *Chlamydomonas* axonemes (Whitman, 1986) monitored by video-enhanced differential interference contrast (VE-DIC) microscopy. Using a modified protocol of Walker *et al.* (1988), yeast tubulin (1.4 μM) in filter-sterilized PEM (100 mM Pipes, 1 mM EGTA, 1 mM MgSO$_4$, pH 6.9) supplemented with 0.5 mM GTP, was incubated in the sealed perfusion chamber on the microscope slide for 30 min at 30°C to achieve steady state. Images of microtubules were recorded for no longer than 90 min after steady state was achieved. Thirty-two wild-type and 16 tub2p-C354S microtubules were analyzed using the RTM software kindly provided by E. D. Salmon (University of North Carolina). Length measurements were recorded every 30–45 s over the lifetime of the microtubule or, in the case of rapid depolymerization, as often as possible (2–3 s^{-1}). For wild-type microtubules, all growth phases lasted >7 min, with a time-averaged growth rate > 7.8 μm/h, and shortening rates were >3.6 mm/h. For tub2p-C354S microtubules, all growth phases had time-averaged growth rates > 1.8 μm/h, and pauses were >10 min with time-averaged

Figure 1. Tub2-C354 mutants contain one cytoplasmic microtubule. (A) The number of cytoplasmic microtubules per spindle pole body determined by GFP-Tub1p fluorescence for wild-type (black), *tub2-C354S* (gray), and *tub2-C354A* (open) mutant strains: n = 21, 12, 36, and 30 for wild-type; 52, 29, 58, and 42 for *tub2-C354S*; and 36, 14, 68, and 32 for *tub2-C354A* spindle pole bodies in unbudded, small-budded, preanaphase, and anaphase cells, respectively. (B–I) Fluorescent intensity line scan analysis of wild-type (B–D), *tub2-C354S* shown in Figure 2 (E) and Figure 3 (F and G), and *tub2-C354A* (H and I) cytoplasmic microtubules. The fluorescent image used is shown in the top left, and the microtubule represented in the line scan graph (right) is designated by the hatched bar in the identical fluorescent image in the bottom left of each panel. (B and C) Wild-type line scans of consistent intensity. (D) Wild-type line scan in which the intensity decreases by 50%, likely representing two microtubules. (E–I) *tub2-C354* mutant microtubules have approximately uniform intensity, likely representing single microtubules.

length changes of $< \pm 0.6$ μm/h. For tub2p-C354S microtubules, shortening rates were >180 μm/h. Microtubule dynamic parameters were defined and calculated as described for in vivo analysis.

Polymer mass steady state was verified by assembling 1.4 μM tubulin under identical conditions with the same concentration of purified axonemes. At time points between 15 and 120 min, aliquots were analyzed by a microtubule sedimentation assay. The amount of polymer was constant through 120 min of incubation for both wild-type and tub2p-C354S tubulin.

RESULTS

A Single Stable Cytoplasmic Microtubule Facilitates Spindle Positioning

Wild-type cells typically contain several cytoplasmic microtubules as visualized with GFP-Tub1p. Unbudded and small-budded wild-type cells contained an average of 2.7 $\pm$ 0.9 and 3.2 $\pm$ 1.2 cytoplasmic microtubules, respectively. The majority of cells transformed with *tub2-C354S* or *tub2-C354A* in place of wild-type *TUB2* contained only a single cytoplasmic microtubule emanating from the spindle pole body (Figure 1A). *Tub2-C354S* mutants contained 1.1 $\pm$ 0.3

and 1.1 $\pm$ 0.4, whereas *tub2-C354A* mutants contained 1.3 $\pm$ 0.5 and 1.1 $\pm$ 0.4 cytoplasmic microtubules in unbudded and small-budded cells, respectively (p $<$ 0.001 for all vs. wild-type). During anaphase, 1.0 $\pm$ 0.3 microtubules emanated from each of the duplicated spindle pole bodies in both *tub2-C354* mutants (p $<$ 0.003 for both mutants vs. 1.4 $\pm$ 0.3 for wild-type). The number of cytoplasmic microtubules in wild-type and *tub2-C354* mutants was statistically indistinguishable during preanaphase (Figure 1A). We used line scan analysis to determine whether the structure in the mutants was indeed one microtubule or a perhaps a bundle of a few microtubules (Figure 1, B–I). The constancy of the intensity throughout the structure is indicative of a single microtubule. The decrease in intensity at the tip is observed in wild-type and mutant microtubules.

Cytoplasmic microtubules in unbudded cells pivot around the spindle pole body, and this movement may facilitate localization of the incipient bud site. The single microtubule in *tub2-C354* mutant cells, which underwent infrequent and minor length changes (discussed later), exhibited a similar type of pivoting from the spindle pole body as wild-type microtubules (Figure 2B). By the time an
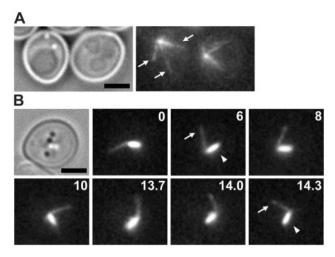
Figure 2. Cytoplasmic microtubule movements in unbudded *tub2-C354* mutant cells. Two-dimensional composite views of the 5 *z*-series fluorescent images are presented following the corresponding transmitted light image. (A) Wild-type cells typically contain several cytoplasmic microtubules (arrows) emanating from the spindle pole body. (B) The single cytoplasmic microtubule (arrow) in the *tub2-C354S* mutant cell undergoes swiveling and pivoting movements without changes in overall microtubule length. The remnant half-spindle (arrowhead) from the previous mitosis can also be seen extending from the area of the spindle pole body. The apparent length of the microtubule and spindle remnant varies due to rotations about the *z*-axis. The mutant cell remained unbudded throughout the time-lapse sequence. Numbers represent elapsed time (min). Bar, 2 μm.

emerging bud was visible by transmitted light microscopy, the microtubule was stationary, with the tip extending into the bud. As the bud grew, the microtubule remained ori-

ented in the bud (Figure 3). The microtubule shortened, with the microtubule tip remaining in the bud, thereby positioning the spindle adjacent to the bud neck (Figure 3).

To determine the fidelity of spindle positioning, we measured the distance from the bud-proximal spindle pole body to the center of the bud neck ~1 min before anaphase B (spindle length > 2 μm). In wild-type cells, the spindle was located 0.83 ± 0.60 μm (n = 9) from the bud neck. Spindles were located 1.27 ± 0.70 (n = 13) and 0.93 ± 0.76 μm (n = 15) from the bud neck in *tub2-C354S* and *tub2-C354A* mutant cells, respectively. Despite the larger average spindle-to-neck distance in the mutant cells, the differences between the strains were statistically indistinguishable (p = 0.13 and 0.74 for wild-type vs. tub2-C354S and *tub2-C354A,* respectively).

Although the spindle was positioned near the bud neck at the time of spindle elongation, the mutant cells displayed defects in spindle orientation before anaphase onset. In wild-type cells, the preanaphase spindle was aligned within 30° of the mother-daughter axis 87% of the time. The preanaphase spindle was greater than 30° offset from the mother-daughter axis 51% of the time in *tub2-C354S* cells and 28% of the time in *tub2-C354A* cells.

Cytoplasmic Microtubule Dynamics in tub2-C354 Mutant Cells

All parameters of microtubule dynamics were severely depressed in *tub2-C354* mutant GI cells (Table 1). Dynamic rates of *tub2-C354* mutant microtubules were statistically different from the corresponding rates for wild-type microtubules (p < 0.001). Growth and shrinkage rates were decreased by 83–92% compared with wild-type microtubules. The *tub2-C354* mutant microtubules had transition frequencies that were 2–5% of those for wild-type microtubules and spent the great majority of the time in the paused state
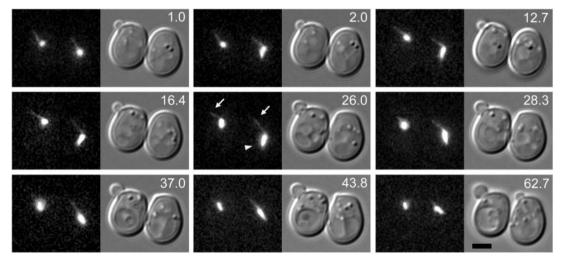

Figure 3. Cytoplasmic microtubules in *tub2-C354* mutant cells remain oriented and depolymerize toward the growing bud. The microtubule (arrows) in the left cell remained oriented toward the bud for ~30 min before becoming too short to reliably identify. The microtubule in the right cell is continuously oriented toward the incipient bud site for 30 min before bud emergence is visible. Both microtubules reached lengths of ~2 μm before depolymerizing to <0.5 μm. Note that spindle pole body migration to the bud neck accompanies microtubule depolymerization. Two-dimensional composite views of the 5 *z*-series fluorescent images are presented next to the corresponding DIC image. Numbers represent elapsed time (min). Bar, 2 μm.

Table 1. In vivo cytoplasmic microtubule dynamic rates and frequencies[a]

	Wild-type	*tub2-C354S*	*tub2-C354A*
Growth rate (μm/min)			
Unbudded cells	1.66 ± 0.54 (31)	0.29 ± 0.16 (4)	0.13 ± 0.02 (4)
Small-budded cells	1.33 ± 0.52 (11)	0.29 ± 0.13 (5)	NA[b] (0)
Preanaphase cells	1.30 ± 0.42 (28)	0.23 ± 0.11 (9)	NA[b] (0)
Anaphase cells	1.31 ± 0.41 (15)	0.40 ± 0.20 (24)	0.12 ± 0.04 (8)
Shrinkage rate (μm/min)			
Unbudded cells	2.66 ± 0.77 (34)	0.46 ± 0.21 (6)	0.28 ± 0.03 (3)
Small-budded cells	2.24 ± 0.54 (9)	0.31 ± 0.23 (9)	0.27 ± 0.18 (6)
Preanaphase cells	1.98 ± 0.68 (30)	0.42 ± 0.18 (9)	0.15 (1)
Anaphase cells	1.89 ± 0.74 (18)	0.49 ± 0.21 (15)	0.31 ± 0.20 (2)
Catastrophe frequency (min^{-1})			
Unbudded cells	0.52 ± 0.10 (28)	0.012 ± 0.005 (5)	0.012 ± 0.007 (3)
Small-budded cells	0.45 ± 0.15 (9)	0.036 ± 0.014 (7)	0.036 ± 0.016 (5)
Preanaphase cells	0.46 ± 0.10 (24)	0.024 ± 0.009 (7)	0.006 (1)
Anaphase cells	0.25 ± 0.08 (10)	0.072 ± 0.021 (12)	0.012 ± 0.008 (2)
Rescue frequency (min^{-1})			
Unbudded cells	0.26 ± 0.09 (14)	0.006 ± 0.004 (3)	0.012 ± 0.007 (3)
Small-budded cells	0.15 ± 0.08 (3)	0.018 ± 0.009 (4)	<0.006 (0)[b]
Preanaphase cells	0.21 ± 0.07 (11)	0.036 ± 0.012 (9)	<0.005 (0)[b]
Anaphase cells	0.22 ± 0.07 (9)	0.108 ± 0.025 (18)	0.024 ± 0.011 (5)
Dynamicity (dimers/s)			
Unbudded cells	49.1	0.99	0.52
Small-budded cells	35.9	3.48	1.96
Preanaphase cells	33.1	1.49	0.25
Anaphase cells	25.4	5.90	1.26

[a] In wild-type cells 10 to 25 microtubules were analyzed. In *tub2-C354S* cells, 8 to 16 microtubules were analyzed. In *tub2-C354A* cells 5 to 15 microtubules were analyzed. Results are reported as the mean ± 1 SD. The number of events is in parentheses.
[b] No events were observed during the total time analyzed.

(Tables 1 and 2). The dynamicity of the *tub2-C354S* microtubules was 2% that of wild-type microtubules, and the *tub2-C354A* mutation produced microtubules with 1% the dynamicity of wild-type microtubules (Table 1). In 700 min of observation none of the microtubule depolymerizations in

Table 2. Time distribution of in vivo microtubule dynamic phases[a]

	Wild-type	*tub2-C354S*	*tub2-C354A*
Time spent in growth (%)			
Unbudded cells	47.5	3.3	7.5
Small-budded cells	50.7	5.6	0.0[b]
Preanaphase cells	40.5	9.8	0.0[b]
Anaphase cells	29.3	31.5	25.8
Time spent in shrinkage (%)			
Unbudded cells	35.2	3.5	2.2
Small-budded cells	25.8	33.1	23.2
Preanaphase cells	31.4	7.1	2.2
Anaphase cells	26.1	17.0	2.8
Time spent attenuated (%)			
Unbudded cells	17.3	93.2	90.3
Small-budded cells	23.5	61.4	76.8
Preanaphase cells	28.1	83.0	97.8
Anaphase cells	44.6	51.4	71.4

[a] The data come from the experiments described in Table 1.
[b] No growth events were observed.

the mutant unbudded cells resulted in the microtubule becoming <1 μm in length. By contrast, in 53 min of observation 22 of the 25 wild-type microtubules analyzed in unbudded cells underwent length excursions < 1 μm.

The parameters of microtubule dynamics in the mutant cells were altered during the cell cycle in a different manner than in wild-type cells (Table 1). For example, the growth and shrinkage rates in wild-type cells were lower in anaphase than in unbudded cells, but in the mutants these parameters did not change significantly during the cell cycle. On the other hand, microtubules in the mutants showed much more dramatic changes in transition frequencies, proportion of time spent in each phase, and dynamicity. For example, in the *tub2-C354S* mutant there was a 6-fold difference in catastrophe and an 18-fold difference in rescue frequency between unbudded and anaphase cells. In addition, the pattern of cell cycle–dependent microtubule dynamics modulation differed in the mutant cells. Wild-type microtubules were most dynamic in unbudded cells and became progressively less dynamic throughout the cell cycle, decreasing in dynamicity by 49% between unbudded and anaphase cells. In the mutant cells, microtubules were least dynamic in unbudded and preanaphase cells, and dynamicity was stimulated as much as fourfold and sixfold in small-budded and anaphase cells, respectively. In both mutants, the increased microtubule dynamicity in small-budded cells was effected by a 3-fold increase in catastrophe frequency and a 10-fold increase in the proportion of time

Figure 4. Cytoplasmic microtubule dynamic behavior in wild-type and *tub2-C354* mutant cells. Representative lifetime history plots constructed from three-dimensional length measurements (see MATERIALS AND METHODS) are presented. The length axis is identical for all plots. Note the scale of the time axis is different for wild-type and mutant microtubules. (A) Microtubules in unbudded wild-type cells undergo several length excursions in <300 s. (B) Microtubules in unbudded *tub2-C354* mutant cells are relatively nondynamic for as long as 3500 s. (C) In small-budded *tub2-C354* mutants, dynamicity is increased nearly fourfold relative to unbudded cells and microtubules undergo net depolymerization. (D) In preanaphase cells, *tub2-C354* mutant microtubules are again relatively nondynamic. (E) During anaphase, dynamicity is up to sixfold higher than in unbudded cells and *tub2-C354* mutant microtubules undergo net polymerization. Panels B–E show representative lifetime history plots of either *tub2-C354A* or *tub2-C354S* microtubules.

spent shrinking, which resulted in overall shortening of the cytoplasmic microtubule. Conversely, rescue frequency was increased to about twice that of the catastrophe frequency in anaphase cells, and in the case of the *tub2-C354S* mutant, was accompanied by a 10-fold increase in the percent time spent growing, resulting in net elongation of the cytoplasmic microtubule during anaphase.

Representative lifetime histories of microtubules in wild-type and mutant cells are presented in Figure 4. The difference between wild-type and mutant microtubules is readily apparent. Although microtubules in the wild-type strain underwent several transitions within 300 s, those in the mutant strains were mostly paused for up to 3500 s. Additionally, the data in Figure 4 demonstrate that the mutant

microtubules typically underwent net disassembly in small-budded cells, were relatively nondynamic in unbudded and preanaphase cells, and underwent net growth in anaphase cells. *Tub2-C354* mutant cells completed anaphase with a single cytoplasmic microtubule on each spindle pole body. These microtubules had elongated during anaphase and remained long and stable during the subsequent G1 phase.
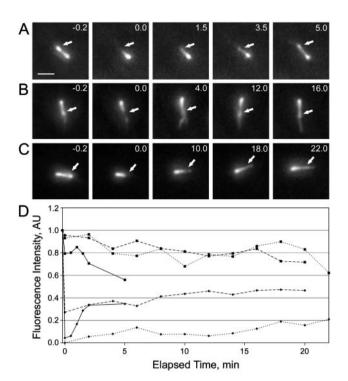
Spindle Microtubule Dynamics

The mitotic spindle, consisting of kinetochore and interpolar microtubules, is typically disassembled within a few minutes of the completion of anaphase (Maddox *et al.*, 2000; Pearson *et al.*, 2001). The kinetochore microtubules depolymerize during anaphase A (Winey *et al.*, 1995), and the interpolar microtubules separate at the midzone and depolymerize toward the spindle poles during telophase (Maddox *et al.*, 2000). In the *tub2-C354* mutants, the mitotic spindle failed to depolymerize after spindle separation in the midzone, and a remnant half-spindle was visible as a fluorescent tuft extending from the spindle pole body (Figure 2). Therefore, the mutant unbudded and small-budded cells contained remnant spindle microtubules from the previous mitosis. The spindle microtubules in the mutants typically depolymerized before spindle assembly in the ensuing cell cycle.

To determine if the *tub2-C354* mutations affect spindle microtubule dynamics, we measured the spindle tubulin turnover rate in these mutants. Measurement of the dynamics of individual microtubules in the yeast spindle is not possible because of the high density of microtubules within the mitotic spindle. However, FRAP of GFP-Tub1p–labeled spindle microtubules can be used to measure the turnover of tubulin within the mitotic spindle. Previous studies have shown that spindle microtubules in wild-type cells turnover with a half-life of approximately 1 min (Maddox *et al.*, 2000). This turnover is likely due to the dynamic instability of kinetochore microtubules growing and shortening at their plus ends.

To measure the turnover of GFP-Tub1p in the mutant spindle, we photobleached half of the mitotic spindle and then monitored the recovery of the bleached half-spindle fluorescence intensity and the decrease of the unbleached half-spindle fluorescence intensity (Figure 5). The *tub2-C354S* mutant showed a first-order rate constant (k) of 0.0026 ± 0.0016 and a corrected recovery (R) of 0.44 ± 0.17 after 17.6 min; which is 15% of the rate and 32% less recovery than that recorded for wild-type cells ($k = 0.0174 \pm 0.0113$ and $R = 0.65 \pm 0.24$ after 2 min; Figure 5; Table 3). The *tub2-C354A* mutant showed a more severe phenotype with a first-order rate constant (k) of 0.0014 ± 0.0009 and a corrected recovery (R) of 0.44 ± 0.23 after 18.6 min, only 8% of the rate and 32% less recovery than wild-type cells (Figure 5; Table 3). These results indicate that the *tub2-C354* mutations substantially decrease the rate and total turnover of GFP-tubulin within the mitotic spindle. The reduced recovery in the mutants may reflect the limited duration of the analysis, even though it was 10 times longer than that needed for maximum wild-type recovery or a stable population of spindle microtubules.

Spindles in our wild-type strain reached an average length of >8 μm before spindle separation and breakdown occurred. In the *tub2-C354S* mutant, the average spindle

Figure 5. Spindle microtubule turnover in *tub2-C354* mutants. (A) FRAP of a wild-type half-spindle. (B) FRAP of a *tub2-C354S* half-spindle. (C) FRAP of a *tub2-C354A* half-spindle. Arrows indicate bleached half-spindles. A, B, and C time point −0.2 min describes the spindle before photobleaching, and 0.0 min shows the spindle immediately post laser exposure. The time points after laser exposure were performed using 3D time lapse imaging for the indicated timeframe. The control shows rapid recovery (A; arrows), whereas the two mutants show decreased rates and total percent recovery (B and C; arrows). (D) Quantitation of the fluorescence recovery for wild-type (solid lines), *tub2-C354S* (dashed lines), and *tub2-C354A* (dotted lines) with the bleached (diamonds) and unbleached (squares) half-spindle fluorescence intensities. Numbers represent elapsed time (min). Scale bar, 2 μm.

length was 5.1 ± 0.73 μm (n = 23, p < 0.001 vs. wild-type) at the time of spindle midzone separation and 17% of *tub2-C354S* spindles separated before reaching a length of 4.5 μm. The average length of a *tub2-C354A* mutant spindle at the time of spindle midzone separation was only 4.5 ± 0.98 μm (n = 20, p < 0.001 vs. wild-type, p = 0.016 vs. tub2-C354S), and 55% of the spindles separated before reaching 4.5 μm in length. In fact, 45% of *tub2-C354A* spindles separated when the spindle was between 3 and 4 μm long.

The rate of spindle elongation can be used to monitor the dynamics of polar microtubules (Straight *et al.*, 1998; Severin *et al.*, 2001). In budding yeast, spindle elongation during anaphase is biphasic (Kahana *et al.*, 1995; Yeh *et al.*, 1995; Straight *et al.*, 1997). In our wild-type strain the initial elongation rate was 0.73 μm/min, dropping to 0.22 μm/min at a spindle length of 4 μm (Table 3). Many of the spindles in the mutant strains separated before reaching lengths greater than ~4.5 μm; however, a significant number reached lengths sufficient to allow us to determine the rate of elongation for spindles >4 μm long. The rates of spindle elon-

Table 3. Spindle elongation rates and FRAP parameters in wild-type and *tub2-C354* mutants
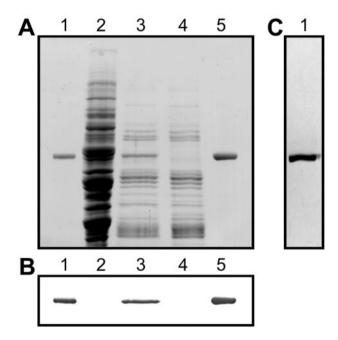
	Wild-type	*tub2-C354S*	*tub2-C354A*
Elongation rate (μm/min)			
Initial (fast) phase[a]	0.73 ± 0.10 (7)	0.27 ± 0.09 (12)	0.17 ± 0.08 (13)
Sequential (slow) phase[b]	0.22 ± 0.08 (7)	0.16 ± 0.06 (8)	0.05 ± 0.01 (3)
FRAP parameters[c]			
First-order rate constant	0.0174 ± 0.0113 (9)	0.0026 ± 0.0016 (7)	0.0014 ± 0.0009 (7)
Half-time to recovery, s	52 ± 24 (9)	354 ± 186 (7)	600 ± 236 (7)
Corrected recovery (R)	0.65 ± 0.24 (8)	0.44 ± 0.17 (7)	0.44 ± 0.23 (7)

Results are reported as the mean ± 1 SD. Number of events is in parentheses.

[a] Elongation rates for spindles between 2 and 4 μm long.

[b] Elongation rates for spindles greater than 4 μm long.

[c] FRAP parameters were determined by analyzing an average recovery period after photobleaching of 2, 18, and 19 min for wild-type, *tub2-C354S*, and *tub2-C354A* spindles, respectively. The corrected recovery is the ratio of the fluorescence intensity of the bleached pole to the unbleached pole after recovery.

gation were significantly lower in the *tub2-C354* mutants; however, both strains displayed biphasic spindle elongation kinetics (Table 3). The *tub2-C354S* spindles had rates of 0.27 and 0.16 μm/min for the fast and slow phases of anaphase B, respectively. For the *tub2-C354A* spindles these rates were 0.17 and 0.05 μm/min, respectively. These results indicate that suppression of microtubule dynamics reduces the overall rates of spindle elongation, thought to be driven by microtubule motors (Straight *et al.*, 1998). However, the biphasic properties of spindle elongation are inherent to the process and not the polymer.

In Vitro Dynamics of Wild-type and tub2p-C354S Microtubules

To determine whether the effect of the *tub2-C354* mutations on microtubule dynamics in vivo was solely attributable to the mutated tubulin molecule, we measured the in vitro dynamic parameters of individual microtubules formed from purified wild-type and *tub2-C354S* tubulins. We made use of His$_6$-tag affinity chromatography to purify tubulin from each strain that was homogeneous by SDS-PAGE analysis (Figure 6). The data summarized in Table 4 show clearly that microtubules formed from *tub2-C354S* tubulin are much less dynamic than microtubules formed from wild-type tubulin. Sample microtubule lifetimes are presented in Figure 7. Both types of microtubules spent a very small amount of the total time in the shortening phase. Wild-type microtubules spent almost 100% of the time in the growth phase, whereas tub2p-C354S microtubules spent about half the time in the paused phase. In addition to this difference, the growth and shortening rates of the mutated microtubules were 33 and 6%, respectively, of the corresponding rates for wild-type microtubules. Dynamicity was reduced by 90%. The mutation also reduced the catastrophe frequency and increased the rescue frequency substantially. Wild-type microtubules experienced a catastrophe, on average, every 21.5 min. Tub2p-C354S microtubules experienced a catastrophe, on average, every 130 min (Table 4). Of the four catastrophes recorded for tub2p-C354S microtubules, three were followed by a rescue event. By contrast, wild-type microtubules showed no rescue events after 20 catastrophes. In Figure 7C

the sample lifetimes are presented over a shorter time period and clearly show the differences in the catastrophes of wild-type and tub2p-C354S microtubules.

Figure 6. SDS-PAGE gels and Western blot of yeast tubulin. (A) Coomassie Blue–stained SDS-PAGE gel of purified tubulin from MGY1. Lane 1, 0.5 μg yeast tubulin standard; lane 2, 25 μg 100,000 × g supernatant; lane 3, 10 μg DE52 eluate; lane 4, 10 μg Ni-NTA pass-through; lane 5, 1 μg Ni-NTA eluate. (B) Western-blot of gel shown in A. Staining was with the anti–α-tubulin antibody clone B-5–1-2 and a horseradish peroxidase–conjugated anti-mouse antibody as the secondary antibody (Sigma-Aldrich, St. Louis, MO). Detection was accomplished with 4-chloro-1-napthol and H$_2$O$_2$. Because of its low concentration in the 100,000 × g supernatant, tubulin could not be detected in this fraction. (C) Coomassie Blue–stained SDS-PAGE gel loaded with 2 μg of purified tubulin from MGY1-C354S.

Table 4. In vitro dynamics of wild-type and *tub2-C354S* microtubules[a]

	Wild-type	*tub2-C354S*
Time spent in		
Growth phase (%)	99.6	53.5
Shrinkage phase (%)	0.40	0.57
Attenuated phase (%)	0.00	46.0
Total time, min	431	520
Growth rate (μm/h)	10.6 ± 1.9 (32)	3.5 ± 1.2 (14)
Shrinkage rate (μm/min)	102.7 ± 18.4 (22)[b]	6.1 ± 2.1 (11)[b]
Catastrophe (min^{-1})	0.0464 ± 0.010 (20)	0.0077 ± 0.004 (4)
Rescue (min^{-1})	<0.0023[c] (0)	0.0058 ± 0.003 (3)
Dynamicity (dimer/s)	16.6	1.9

[a] For wild-type dynamics 32 microtubules grown from 11 axonemes were analyzed. For *tub2-C354S* dynamics 16 microtubules grown from 8 axonemes were analyzed. Rates and frequencies are reported as the mean $\pm$ 1 SD. The number of events is in parentheses.

[b] Shrinkage events exceed catastrophes due to brief pauses during disassembly (see Figure 7C).

[c] No rescue events were observed for wild-type microtubules in 431 min.

DISCUSSION

In tub2-C354 Mutants a Single Stable Cytoplasmic Microtubule Finds the Bud Site and Facilitates Spindle Positioning, but not Orientation

Wild-type budding yeast cells contain an average of three and as many as six cytoplasmic microtubules in unbudded cells (Shaw *et al.*, 1997b; Tirnauer *et al.*, 1999). In contrast, *tub2-C354* mutant cells contained one stable and persistent cytoplasmic microtubule throughout the entire unbudded phase of cell growth. Microtubule localization to the bud is believed to involve a search and capture mechanism, which relies on microtubule dynamic instability to effectively probe the entire cell cortex (Carminati and Stearns, 1997). This dynamic property of microtubules has been shown to be an efficient mechanism for probing intracellular space (Holy and Leibler, 1994). Another mechanism of microtubule localization to the bud site has been proposed that involves directed-transport of microtubule ends along polarized actin filaments to the bud (Yin *et al.*, 2000). In wild-type cells, cytoplasmic microtubules interact transiently with the future bud site and bud cortex, but the dynamic nature of the microtubules typically results in detachment and depolymerization out of the bud (Adames and Cooper, 2000; Beach *et al.*, 2000). However, in all the *tub2-C354* mutant cells examined, the cytoplasmic microtubule stopped moving and became stationary, with its end in the vicinity of imminent bud growth before bud emergence was visible. The tip of the *tub2-C354* mutant microtubule remained associated with the emerging bud throughout bud growth. Thus, a minimally dynamic microtubule is able to locate the site of future bud growth without the aid of a dynamic instability-based microtubule probing mechanism. The minimum requirement to find the incipient bud site is simply a microtubule that is long enough to interact with the cell cortex. It would seem that the pivoting motion that the cytoplasmic microtubules undergo might be more important in finding the bud site than dynamics. Thus, at least in the *tub2-C354* mutants, the directed-transport mechanism appears responsible for locating the microtubule structure at the bud site, possibly with the help of actin filaments (Theesfeld *et al.*, 1999; Yin *et al.*, 2000).

Defects in spindle position and orientation can be caused by changes in microtubule dynamics (Tirnauer *et al.*, 1999; Kosco *et al.* 2001). In the *tub2-C354* mutants, the spindle was positioned near the bud neck at the onset of anaphase. However, in the mutants the spindle was not oriented properly along the mother-bud axis in a larger percentage of the cells compared with wild-type cells. The single cytoplasmic microtubule was stable throughout G2/M and was ~1 μm in length during preanaphase. The failure of *tub2-C354* mutants to maintain spindle orientation may reflect their inability to maintain cytoplasmic microtubule-cortical interactions at the distal ends of the mother cell and the bud.

Dynamics of Wild-type and tub2p-C354 Microtubules In Vivo and In Vitro

Our previous studies with the *tub2-C354* mutants demonstrated that the mutations produced phenotypes that were consistent with an increase in microtubule stability (Gupta *et al.*, 2001). To examine the effects of these mutations on microtubule stability in more detail, we analyzed microtubule dynamics in both wild-type and *tub2-C354* mutant cells using a GFP-Tub1p fusion protein. The wild-type values we obtained for the microtubule dynamic parameters of growth rate, shrinkage rate, catastrophe frequency, and rescue frequency in wild-type cells were in agreement with those reported by others (Carminati and Stearns, 1997; Shaw *et al.*, 1997b; Tirnauer *et al.*, 1999; Adames and Cooper, 2000; Vogel *et al.*, 2001; Kosco *et al.*, 2001). However, all aspects of microtubule dynamics were drastically reduced in both *tub2-C354* mutants. Consistent with our previous findings (Gupta *et al.*, 2001), the *tub2-C354A* mutation decreased dynamics more than the *tub2-C354S* mutation. Depending on the phase of the cell cycle and the mutant, microtubule growth and shrinkage rates were reduced by 69–92%, catastrophe and rescue frequencies by 51–99%, and dynamicity by 77–99%. In addition, in vivo results suggest that a threshold of microtubule dynamicity is required for proper progression through the cell cycle. The more severe *tub2-C354A* mutant
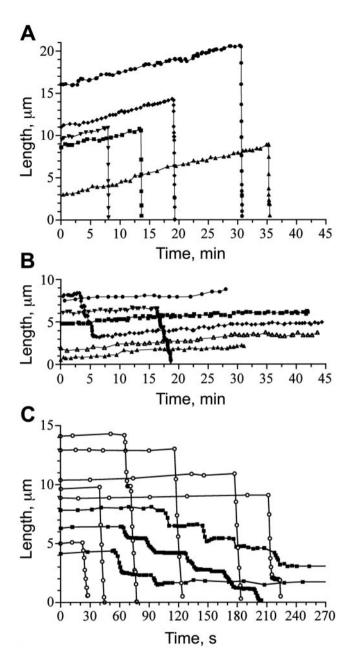
Figure 7. In vitro microtubule dynamic behavior. Representative lifetime history plots are presented for microtubules assembled from (A) wild-type or (B) tub2p-C354S tubulin. The scale is identical in A and B for comparison. Individual microtubules are represented by different symbols in A and B. With wild-type microtubules, no rescue events were observed after 20 catastrophes. However, with tub2p-C354S microtubules, three of the four catastrophe events were followed by a rescue. (C) Six individual wild-type (open circles) and three individual tub2p-C354S (closed squares) catastrophes are superimposed on an expanded time axis for comparison.

displays aneuploidy and decreased viability (Gupta *et al.*, 2001). A minimum dynamicity may therefore be necessary for chromosome or nuclear movement to poles and cortical

sites, respectively, thereby contributing to the fidelity of genome segregation.

Microtubule dynamics in vitro were decreased substantially by the *tub2-C354S* mutation. The changes in in vitro dynamics parameters paralleled those observed in vivo. The one exception was the rescue frequency. The frequency of rescue in vivo was reduced by 50–98% by the *tub2-C354S* mutation. In vitro, however, rescue frequency was increased greater than 2.5-fold in the *tub2-C354S* microtubules. This apparent discrepancy can be explained on the basis of the stability of yeast microtubules. Wild-type microtubules depolymerize very rapidly in vitro, and rescue events are never observed (this study; Davis *et al.*, 1993; Sage *et al.*, 1995a, 1995b). However, the slow depolymerization rate for *tub2-C354S* microtubules in vitro enhanced the opportunity for rescue events, thus explaining the increase in rescue frequency. In contrast, the decreased number of microtubule catastrophes in the mutant cells reduced the opportunity for rescue to occur as well. The large decreases in the frequency of catastrophe and shrinkage rate in vivo and in vitro caused by substituting either a serine or alanine residue for cysteine 354 in Tub2p clearly illustrate the strong stabilizing effect of these mutations on microtubules. Because the in vitro studies were conducted with purified tubulin, the results demonstrate that the extreme microtubule stability is an intrinsic property of the mutated protein. The results further indicate that the intrinsic properties of microtubules are dominant relative to proteins that modulate dynamics in vivo.

Changes in Microtubule Dynamics During the Cell Cycle

The *tub2-C354* mutants provide the most dramatic example to date of cell cycle–specific modulation of microtubule dynamics in budding yeast. Microtubule dynamicity varied as much as 6- to 8-fold during the cell cycle in these cells. The majority of microtubule dynamics modulation occurred because of changes in transition frequencies (up to 18-fold) and the proportion of time spent growing or shrinking (up to 10-fold in each case). These results indicate that microtubule dynamics can be altered to produce either net disassembly (small-budded) or net assembly (late-anaphase) of cytoplasmic microtubules. The decrease in length of the single microtubule in small-budded cells indicates that microtubule depolymerization is responsible for nuclear migration to the bud neck (Adames and Cooper, 2000; Beach *et al.*, 2000).

In the wild-type cells, cytoplasmic microtubules became progressively less dynamic and more persistent as the cells approached mitosis. We found microtubule dynamicity to be reduced 50% between G1 and anaphase (Table 1). This was achieved mainly by about a 25% reduction in growth and shrinkage rates and an increase in the proportion of time microtubules spent paused. The modulation of microtubule dynamics throughout the cell cycle in budding yeast indicates that cellular factors alter the intrinsic dynamic properties of microtubules.

Spindle Dynamics in tub2-C354 Mutant Cells

Spindle microtubule dynamics and the rate and extent of spindle elongation were reduced in the mutants. The results of the quantitative analysis in vivo correspond to the in vitro microtubule dynamics data, indicating that there is no nu-

clear or spindle-specific factor that can override the effects of the tubulin mutation. The anaphase spindles did not reach wild-type lengths (>8 μm), and the second, slower phase of spindle elongation was absent in many of the mutant cells. In the more severe *tub2-C354A* mutant, half of the spindles separated before reaching 4 μm in length. However, the spindle pole bodies segregated properly in all the mitotic events observed. Spindles that elongated significantly beyond 4 μm displayed the same type of biphasic elongation as observed in wild-type strains. In accordance with the less dynamic microtubules, the rates of spindle elongation were correspondingly lower in the *tub2-C354A* mutant relative to the *tub2-C354S* mutant. This finding indicates that the regulation of microtubule dynamics is important in determining the rate of spindle elongation. Previous evidence suggests that microtubule growth rate factors can control the rate of spindle elongation (Masuda and Cande, 1987). Experiments in yeast have shown that the biphasic nature of spindle elongation results from the balanced influence of various microtubule motor proteins (Straight *et al.*, 1998). It is believed that kinesin-like motors influence spindle elongation by generating sliding forces on the interpolar microtubules in the spindle midzone. The results herein indicate that the biphasic rates are dependent on changes in the rate of polar microtubule elongation. The biphasic nature of the mutant spindle kinetics indicates that the balance of factors involved in spindle behavior contribute to the qualitative aspects of spindle elongation, but the restricted microtubule dynamics influences the quantitative rates of elongation. Clearly, the regulation of microtubule dynamics can directly influence microtubule-based processes such as spindle assembly and elongation.

The midanaphase checkpoint has been characterized as a pause in spindle elongation (at ~4 μm in length) in response to DNA damage (Yang *et al.*, 1997), but the mechanism of the midanaphase checkpoint is not understood. Spindle elongation in the *tub2-C354* mutants frequently paused at ~4 μm in length, suggesting possible involvement of the midanaphase checkpoint. However, the fact that the short *tub2-C354* mutant spindles separated prematurely rather than remaining paused or elongating suggests an alternative explanation: that the difficulties observed in spindle elongation are structural and result from stabilized microtubules. In addition to the midanaphase checkpoint, the biphasic transition separates periods of spindle elongation that are controlled by different cellular factors, e.g., Cin8p and Kip1p (Straight *et al.*, 1998), and may represent fundamentally different mechanisms of microtubule-based spindle elongation. The *tub2-C354* mutant microtubules may be less capable of performing the functions associated with the second phase of spindle elongation.

C354 in β-Tubulin and Microtubule Dynamics

The dynamicity of microtubules varies according to the species (Davis *et al.*, 1993; Detrich *et al.*, 2000) and the isotype of tubulin within a species (Panda *et al.*, 1994; Gonçalves *et al.*, 2001). Such variations are due to multiple differences in amino acid sequences. Our results demonstrate the sensitivity of microtubule dynamics to a single change in the primary sequence of tubulin, a point that has also been demonstrated with mutations of putative GTP binding site residues (Sage *et al.*, 1995a, 1995b; Anders and Botstein, 2001;

Dougherty *et al.*, 2001). C354 in β-tubulin is situated at the α,β-dimer interface and is unlikely to be directly involved in longitudinal or lateral interactions in microtubule protofilaments. In our previous article we speculated that the mutation at C354 might produce a change in the structure of the tubulin dimer that could translate into stronger interprotofilament interactions in the microtubule (Gupta *et al.*, 2001). This residue appears to be located at or near the colchicine binding site (Bai *et al.*, 1996). It has been proposed that colchicine and other antimitotic drugs that modify microtubule dynamics mimic naturally occurring compounds that regulate microtubule function (Wilson and Jordan, 1995). The activities of microtubule regulatory agents that bind to the colchicine site may be mediated through contacts with C354 in β-tubulin.

REFERENCES

Adames, N.R., and Cooper, J.A. (2000). Microtubule interactions with the cell cortex causing nuclear movements in *Saccharomyces cerevisiae*. J. Cell Biol. *149*, 863–874.

Anders, K.R., and Botstein, D. (2001). Dominant-lethal α-tubulin mutants defective in microtubule depolymerization in yeast. Mol. Biol. Cell *12*, 3973–3986.

Bai, R.-l., Lin, C.M., Nguyen, N.Y., Liu, T.-Y., and Hamel, E. (1989). Identification of the cysteine residue of β-tubulin alkylated by the antimitotic agent 2,4-dichlorobenzyl-thiocyanate, facilitated by separation of the protein subunits of tubulin by hydrophobic column chromatography. Biochemistry *28*, 5606–5612.

Bai, R., Pei, X-Y., Boyé, O., Getahun, Z., Grover, S., Bekisz, J., Nguyen, N.Y., Brossi, A., and Hamel, E. (1996). Identification of cysteine 354 of β-tubulin as part of the binding site for the A ring of colchicine. J. Biol. Chem. *271*, 12639–12645.

Bai, R., Ewell, J.B., Nguyen, N.Y., and Hamel, E. (1999). Direct photoaffinity labeling of cysteine 211 or a nearby amino acid residue of β-tubulin by guanosine 5′-diphosphate bound in the exchangeable site. J. Biol. Chem. *274*, 12710–12714.

Barnes, G., Louie, K.A., and Botstein, B. (1992). Yeast proteins associated with microtubules in vitro and in vivo. Mol. Biol. Cell *3*, 29–47.

Beach, D.L., Thibodeaux, J., Maddox, P., Yeh, E., and Bloom, K. (2000). The role of the proteins Kar9 and Myo2 in orienting the mitotic spindle of budding yeast. Curr. Biol. *10*, 1497–1506.

Bradford, M.M. (1976). A rapid and sensitive method for the quantitation of microgram quantities of protein utilizing the principle of protein dye-binding. Anal. Biochem. *72*, 248–254.

Carminati, J.L., and Stearns, T. (1997). Microtubules orient the mitotic spindle in yeast through dynein-dependent interactions with the cell cortex. J. Cell Biol. *138*, 629–641.

Davis, A., Sage, C., Wilson, L., and Farrell, K.W. (1993). Purification and biochemical characterization of tubulin from the budding yeast *Saccharomyces cerevisiae*. Biochemistry *32*, 8823–8835.

Detrich, H.W., III, Parker, S.K., Williams, R.C., Jr., Nogales, E., and Downing, K.H. (2000). Cold adaptation of microtubule assembly and disassembly. Structural interpretation of primary sequence changes present in the α- and β-tubulins of Antarctic fishes. J. Biol. Chem. 47, 37038–37047.

Dhamodharan, R., and Wadsworth, P. (1995). Modulation of microtubule instability in vivo by brain microtubule associated proteins. J. Cell Sci. 108, 1679–1689.

Dougherty, C.A., Sage, C.A., Davis, A., and Farrell, K.W. (2001). Mutation in the β-tubulin signature motif suppresses microtubule GTPase activity and dynamics and slows mitosis. Biochemistry 40, 15725–15732.

Drechsel, D.N., Hyman, A.A., Cobb, M.H., and Kirschner, M.W. (1992). Modulation of the dynamic instability of tubulin assembly by the microtubule-associated protein tau. Mol. Biol. Cell 3, 1141–1154.

Erickson, H.P., and O'Brien, T. (1992). Microtubule dynamic instability and GTP hydrolysis. Annu. Rev. Biophys. Biomol. Struct. 21, 145–166.

Gonçalves, A., Braguer, D., Kamath, K., Martello, L., Briand, C., Horwitz, S., Wilson, L., and Jordan, M.A. (2001). Resistance to taxol in lung cancer cells associated with increased microtubule dynamics. Proc. Natl. Acad. Sci. USA 98, 11737–11741.

Gupta, M.L., Jr., Bode, C.J., Dougherty, C.A., Marquez, R.T., and Himes, R.H. (2001). Mutagenesis of β-tubulin cysteine residues in Saccharomyces cerevisiae: mutation of cysteine 354 results in cold-stable microtubules. Cell Motil. Cytoskeleton 49, 67–77.

Hamill, D.R., Howell, B., Cassimeris, L., and Suprenant, K.A. (1998). Purification of a WD repeat protein EMAP, that promotes microtubule dynamics through an inhibition of rescue. J. Biol. Chem. 273, 9285–9291.

Holy, T.E., and Leibler, S. (1994). Dynamic instability of microtubules as an efficient way to search in space. Proc. Natl. Acad. Sci. USA. 91, 5682–5685.

Huffaker, T.C., Thomas, J.H., and Botstein, D. (1988). Diverse effects of β-tubulin mutations on microtubule formation and function. J. Cell Biol. 106, 1997–2010.

Hunter, A.W., and Wordeman, L. (2000). How motor proteins influence microtubule polymerization dynamics. J. Cell Sci. 113, 4379–4389.

Jayaram, B., and Haley, B.E. (1994). Identification of peptides within the base binding domains of the GTP- and ATP-specific binding sites of tubulin. J. Biol. Chem. 269, 3233–3242.

Kahana, J.A., Schnapp, B.J., and Silver, P.A. (1995). Kinetics of spindle pole body separation in budding yeast. Proc. Natl. Acad. Sci. USA 92, 9707–9711.

Kowalski, R.J., and Williams, R.C., Jr. (1993). Microtubule-associated protein 2 alters the dynamic properties of microtubule assembly and disassembly. J. Biol. Chem. 268, 9847–9855.

Kosco, K.A., Pearson, C.G., Maddox, P.S., Wang, P.J., Adams, I.R., Salmom, E.D., Bloom, K., and Huffaker, T.C. (2001). Control of microtubule dynamics by Stu2p is essential for spindle orientation and metaphase chromosome alignment in yeast. Mol. Biol. Cell 12, 2870–2880.

Ludueña, R.F., and Roach, M.C. (1991). Tubulin sulfhydryl groups as probes and targets for antimitotic and antimicrotubule agents. Pharmac. Ther. 49, 133–152.

Maddox, P.S., Bloom, K.S., and Salmon, E.D. (2000). The polarity and dynamics of microtubule assembly in the budding yeast Saccharomyces cerevisiae. Nat. Cell Biol. 2, 36–41.

Masuda, H., and Cande, W.Z. (1987). The role of tubulin polymerization during spindle elongation in vitro. Cell 49, 193–202.

Mejillano, M.R., Shivanna, B.D., and Himes, R.H. (1996). Studies on the nocodazole-induced GTPase activity of tubulin. Arch. Biochem. Biophys. 336, 130–138.

Mitchison, T., and Kirschner, M. (1984). Dynamic instability of microtubule growth. Nature 312, 237–242.

O'Toole, E.T., Winey, M., and McIntosh, J.R. (1999). High-voltage electron tomography of spindle pole bodies and early mitotic spindles in the yeast Saccharomyces cerevisiae. Mol. Biol. Cell 10, 2017–2031.

Panda, D., Miller, H.P., Banarjee, A., Ludueña, R.F., and Wilson, L. (1994). Microtubule dynamics in vitro are regulated by the tubulin isotype composition. Proc. Natl. Acad. Sci. USA 91, 11358–11362.

Pearson, C.G., Maddox, P.S., Salmon, E.D., and Bloom, K. (2001). Budding yeast chromosome structure, and dynamics during mitosis. J. Cell Biol. 152, 1255–1266.

Sage, C.R., Davis, A.S., Dougherty, C.A., Sullivan, K., and Farrell, K.W. (1995a). beta-Tubulin mutation suppresses microtubule dynamics in vitro and slows down mitosis in vivo. Cell Motil. Cytoskeleton 30, 285–300.

Sage, C.R., Dougherty, C.A., Davis, A.S., Burns, R.G., Wilson, L., and Farrell, K.W. (1995b). Site-directed mutagenesis of putative GTP-binding sites of yeast β-tubulin: evidence that α-, β-, and δ-tubulins are atypical GTPases. Biochemistry 34, 7409–7419.

Severin, F., Habermann, B., Huffaker, T., and Hyman, T. (2001). Stu2 promotes mitotic spindle elongation in anaphase. J. Cell Biol. 153, 435–442.

Shan, B., et al. (1999). Selective covalent modification of β-tubulin residue Cys-239 by T138067, an antitumor agent with in vitro efficacy against multidrug-resistant tumors. Proc. Natl. Acad. Sci. USA 96, 5686–5691.

Shaw, S.L., Yeh, E., Bloom, K., and Salmon, E.D. (1997a). Imaging green fluorescent protein fusion proteins in Saccharomyces cerevisiae. Curr. Biol. 7, 701–704.

Shaw, S.L., Yeh, E., Maddox, P., Salmon, E.D., and Bloom, K. (1997b). Astral microtubule dynamics in yeast: a microtubule-based searching mechanism for spindle and nuclear migration into the bud. J. Cell Biol. 139, 985–984.

Shivanna, B.D., Mejillano, M.R., Williams, T.D., and Himes, R.H. (1993). Exchangeable GTP binding site of β-tubulin. J. Biol. Chem. 268, 127–132.

Straight, A.F., Marshall, W.F., Sedat, J.W., and Murray, A.W. (1997). Mitosis in living budding yeast: anaphase A but no metaphase plate. Science 277, 574–578.

Straight, A.F., Sedat, J.W., and Murray, A.W. (1998). Time-lapse microscopy reveals unique roles for kinesins during anaphase in budding yeast. J. Cell Biol. 143, 687–694.

Theesfeld, C.L., Irazoqui, J.E., Bloom, K., and Lew, D.J. (1999). The role of actin in spindle orientation changes during the Saccharomyces cerevisiae cell cycle. J. Cell Biol. 146, 1019–1031.

Tirnauer, J.S., O'Toole, E.O., Berrueta, L., Bierer, B.E., and Pellman, D. (1999). Yeast Bim1p promotes the G1-specific dynamics of microtubules. J. Cell Biol. 145, 993–1007.

Toso, R.J., Jordan, M.A., Farrell, K.W., Matsumoto, B., and Wilson, L. (1993). Kinetic stabilization of microtubule dynamic instability in vitro by vinblastine. Biochemistry 32, 1285–1293.

Vogel, J., Drapkin, B., Oomen, J., Beach, D., Bloom, K., and Snyder, M. (2001). Phosphorylation of γ-tubulin regulates microtubule organization in budding yeast. Dev. Cell 1, 621–631.

Walczak, C.E. (2000). Microtubule dynamics and tubulin interacting proteins. Curr. Opin. Cell Biol. 12, 52–56.

Walker, R.A., O'Brien, E.T., Pryer, M.F., Soboeiro, W.A., Voter, W.A., Erickson, H.P., and Salmon, E.D. (1988). Dynamic instability of individual microtubules analyzed by video light microscopy: rate constants and transition frequencies. J. Cell Biol. *107*, 1437–1448.

Whitman, G.B. (1986). Isolation of *Chlamydomonas* flagella and flagellar axonemes. Methods Cell Biol. *134*, 280–290.

Wilson, L., and Jordan, M.A. (1995). Microtubule dynamics: taking aim at a moving target. Chem. Biol. *2*, 569–573.

Winey, M., Mamay, C.L., O'Toole, E.T., Mastronarde, D.N., Giddings, T.H., Jr., McDonald, K.L., and McIntosh, R. (1995). Three-dimensional ultrastructure analysis of the *Saccharomyces cerevisiae* mitotic spindle. J. Cell Biol. *129*, 1601–1615.

Yang, S.S., Yeh, E., Salmon, E.D., and Bloom, K. (1997). Identification of a mid-anaphase checkpoint in budding yeast. J. Cell Biol. *136*, 345–354.

Yeh, E., Skibbens, R.V., Cheng, J.W., Salmon, E.D., and Bloom, K. (1995). Spindle dynamics and cell regulation of dynein in the budding yeast. Saccharomyces cerevisiae. J. Cell Biol. *130*, 687–700.

Yin, H., Pruyne, D., Huffaker, T.C., and Bretscher, A. (2000). Myosin V orientates the mitotic spindle in yeast. Nature *406*, 1013–1015.